Two-Dimensional Geoelectrical Modeling Using a Rayleigh-Fourier Method

Ana Osella, Patricia Martinelli, and Daniel Cernadas

***Abstract*—In this paper, we present a new method for DC resistivity modeling as an alternative to finite element and finite difference techniques, based on a Rayleigh-Fourier approach. This is especially adequate to model 2-D layered structures with smooth irregular boundaries.**

The validity of the method is verified by comparing its results with FE solutions for two synthetic models, representing a horst and a graben. The ability to model actual data has also been tested by applying it to interpret data from tectonic basin in the Sierras Pampeanas region in Argentina. During the modeling process, the method showed good convergence and proved friendly to use. Several layers could be identified as being part of an aquifer complex, and the most remarkable fact regarding the reliability of the results is that the description of these layers is in good agreement with information from wells.

***Index Terms*—DC resistivity method, geoelectrical prospecting.**

I. Introduction

DC RESISTIVITY methods are especially adequate to obtain an electrical imaging of the shallow layers. The depth of penetration depends on the geometrical configuration of the electrodes, but usually it can reach down to several hundred meters. The interpretation of the data requires the application of numerical methods to model the geoelectrical structures. A first insight may be achieved assuming a stratified earth, but the complexity of the actual structure makes it necessary to consider 2-D or even 3-D models.

Different methods have been developed to solve these kinds of problems, based on three principal numerical techniques: integral equation approaches [1], [2], finite element methods [3]–[5], and finite diference methods [6]–[10]. Each technique has its own advantage and is suitable for particular electrode configurations and geometries and features of the surveyed area.

In previous papers, we developed an algorithm to model the magnetotelluric response of two-dimensional (2-D) and three-dimensional (3-D) structures composed of homogeneous layers with smooth irregular boundaries, using a Rayleigh-Fourier (RF) technique. Results obtained with these methods were in agreement with the ones obtained by finite elements and finite differences and have proved to be easier to apply when large scale variations are involved [11], [12]. In the present paper, we modify this method in order to model the resistivity response of 2-D structures. We apply it to solve horst and graben structures and compare the results with the ones obtained using a finite element technique [13] and also with the curves assuming a one-dimensional (1-D) behavior.

Manuscript received January 11, 1999; revised December 27, 1999. This work was supported by the Consejo Nacional de Investigaciones Científicas y Técnicas (CONICET) and the University of Buenos Aires, Buenos Aires, Argentina.

A. Osella and P. Martinelli are with the Department of Physics, Faculty of Sciences, Exactas y Naturales, Universidad de Buenos Aires, Buenos Aires, Argentina, and also with the Consejo Nacional de Investigaciones Científicas y Técnicas (CONICET), Buenos Aires, Argentina (e-mail: osella@df.uba.ar).

D. Cernadas is with the Department of Physics, Faculty of Sciences, Exactas y Naturales, Universidad of Buenos Aires, Buenos Aires, Argentina.

Publisher Item Identifier S 0196-2892(00)03923-1.

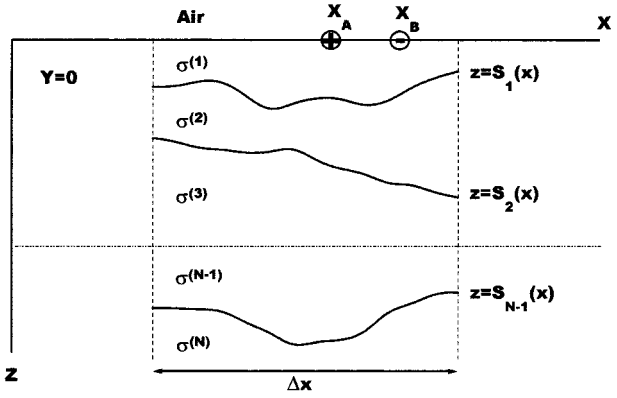

Fig. 1. N-layered structure. x_A and x_B indicate the positions of the current injection electrodes.

II. Theoretical Model

In the formulation, 2-D N-layered structures with irregular boundaries are considered. Such boundaries are described by functions $z = S_n(x)$ for $1 \leq n \leq N-1$. Each medium is linear, homogeneous, and isotropic, and has a conductivity $\sigma^{(n)}$. The current injection electrodes A and B are located along the $y = 0$ profile, at positions x_A and x_B, while the measurement electrodes are positioned at arbitrary positions x_M and x_N, respectively (see Fig. 1).

Inside each layer n and excluding the injection points, the potential function $\phi^{(n)}$ satisfies

$$\nabla^2 \phi^{(n)} = 0 \tag{1}$$

and the current density $\overline{J}^{(n)}$ is obtained from

$$\overline{J}^{(n)} = -\sigma^{(n)} \overline{\nabla} \phi^{(n)}. \tag{2}$$

Here, the problem is solved by developing each potential $\phi^{(n)}$ as a Rayleigh-Fourier series. As some multiple reflections are not included in Rayleigh's scattering theory, the solution actually constitutes an approximation. Validity limits of this approximation have been extensively tested for the magnetotelluric 2-D and 3-D RF methods [11], [12]. In those cases, boundary slopes

up to 50° or 60° (depending on layer resistivities) have been accurately modeled.

To simplify the treatment and without losing generality, it can be assumed that S_n are even and periodic functions of x. The location of the injection electrodes is also made symmetric and periodic in x, and in addition, it is made periodic in y. The periodicity in the x and y coordinates is named λ (Fig. 2). The studied area, located along the $y = 0$ line, corresponds to values of x such that $|x-\lambda/4| \le \Delta X/2$ when $\Delta X/2 < |x-\lambda/4| \le \lambda/4$ the interfaces are 1-D. The effect of these imposed conditions over the zone of interest is negligible when λ is much greater than ΔX.

In the upper layer, the general solution to (1) can be written as

$$\phi^{(1)}(x,y,z) = \phi_S(x,y,z) + \phi_H(x,y,z) \tag{3}$$

where ϕ_S is a source term given by

$$\begin{aligned}\phi_S(x,y,z) = &\frac{I}{2\pi\sigma^{(1)}}\left\{\frac{1}{[(x-x_A)^2+y^2+z^2]^{1/2}}\right.\\ &\left.+\frac{1}{[(x+x_A)^2+y^2+z^2]^{1/2}}\right\}\\ &-\frac{I}{2\pi\sigma^{(1)}}\left\{\frac{1}{[(x-x_B)^2+y^2+z^2]^{1/2}}\right.\\ &\left.+\frac{1}{[(x+x_B)^2+y^2+z^2]^{1/2}}\right\}\end{aligned} \tag{4}$$

and

$$\begin{aligned}\phi_H(x,y,z) = &\sum_{l,m\ge 0}[A_{lm}^{(1)}\exp(K_{lm}z) + B_{lm}^{(1)}\exp(-K_{lm}z)]\\ &\cdot\cos(k_l x)\cos(k_m y)\end{aligned} \tag{5}$$

where I is the current injected to the soil $k_l = 2l\pi/\lambda$, $k_m = 2m\pi/\lambda$, and $K_{lm} = \sqrt{k_l^2+k_m^2}$.

Considering (2), $\overline{J}^{(1)}$ is given by

$$\overline{J}^{(1)}(x,y,z) = \overline{J}_S(x,y,z) + \overline{J}_H(x,y,z) \tag{6}$$

with

$$\begin{aligned}\overline{J}_S(x,y,z) = &\frac{I}{2\pi}\left\{\frac{(x-x_A)\hat{x}+y\hat{y}+z\hat{z}}{[(x-x_A)^2+y^2+z^2]^{3/2}}\right.\\ &\left.+\frac{(x+x_A)\hat{x}+y\hat{y}+z\hat{z}}{[(x+x_A)^2+y^2+z^2]^{3/2}}\right\}\\ &-\frac{I}{2\pi}\left\{\frac{(x-x_B)\hat{x}+y\hat{y}+z\hat{z}}{[(x-x_B)^2+y^2+z^2]^{3/2}}\right.\\ &\left.+\frac{(x+x_B)\hat{x}+y\hat{y}+z\hat{z}}{[(x+x_B)^2+y^2+z^2]^{3/2}}\right\}\end{aligned} \tag{7}$$

and

$$\begin{aligned}&\overline{J}_H(x,y,z)\\ &\quad=\sigma^{(1)}\left\{\sum_{l,m\ge 0} k_l[A_{lm}^{(1)}\exp(K_{lm}z)\right.\\ &\qquad\left.+B_{lm}^{(1)}\exp(-K_{lm}z)]\sin(k_l x)\cos(k_m y)\right\}\hat{x}\\ &\qquad+\sigma^{(1)}\left\{\sum_{l,m\ge 0} k_m[A_{lm}^{(1)}\exp(K_{lm}z)\right.\\ &\qquad\left.+B_{lm}^{(1)}\exp(-K_{lm}z)]\cos(k_l x)\sin(k_m y)\right\}\hat{y}\\ &\qquad-\sigma^{(1)}\left\{\sum_{l,m\ge 0} K_{lm}[A_{lm}^{(1)}\exp(K_{lm}z)\right.\\ &\qquad\left.-B_{lm}^{(1)}\exp(-K_{lm}z)]\cos(k_l x)\cos(k_m y)\right\}\hat{z}\end{aligned} \tag{8}$$

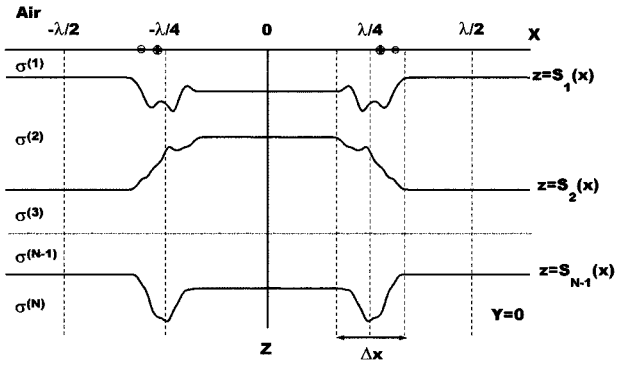

Fig. 2. Extended model used to estimate the geoelectrical response of the structure using the RF approach.

where $\hat{x}$, $\hat{y}$, and $\hat{z}$ are unitary vectors pointing out, respectively, in the directions x, y, and z.

In the other layers, the solutions are

$$\begin{aligned}\phi^{(n)}(x,y,z) = &\sum_{l,m\ge 0}[A_{lm}^{(n)}\exp(K_{lm}z) + B_{lm}^{(n)}\exp(-K_{lm}z)]\\ &\cdot\cos(k_l x)\cos(k_m y)\end{aligned} \tag{9}$$

and

$$\begin{aligned}&\overline{J}^{(n)}(x,y,z)\\ &\quad=\sigma^{(n)}\left\{\sum_{l,m\ge 0} k_l[A_{lm}^{(n)}\exp(K_{lm}z)\right.\\ &\qquad\left.+B_{lm}^{(n)}\exp(-K_{lm}z)]\sin(k_l x)\cos(k_m y)\right\}\hat{x}\\ &\qquad+\sigma^{(n)}\left\{\sum_{l,m\ge 0} k_m[A_{lm}^{(n)}\exp(K_{lm}z)\right.\\ &\qquad\left.+B_{lm}^{(n)}\exp(-K_{lm}z)]\cos(k_l x)\sin(k_m y)\right\}\hat{y}\\ &\qquad-\sigma^{(n)}\left\{\sum_{l,m\ge 0} K_{lm}[A_{lm}^{(n)}\exp(K_{lm}z)\right.\\ &\qquad\left.-B_{lm}^{(n)}\exp(-K_{lm}z)]\cos(k_l x)\cos(k_m y)\right\}\hat{z}.\end{aligned} \tag{10}$$

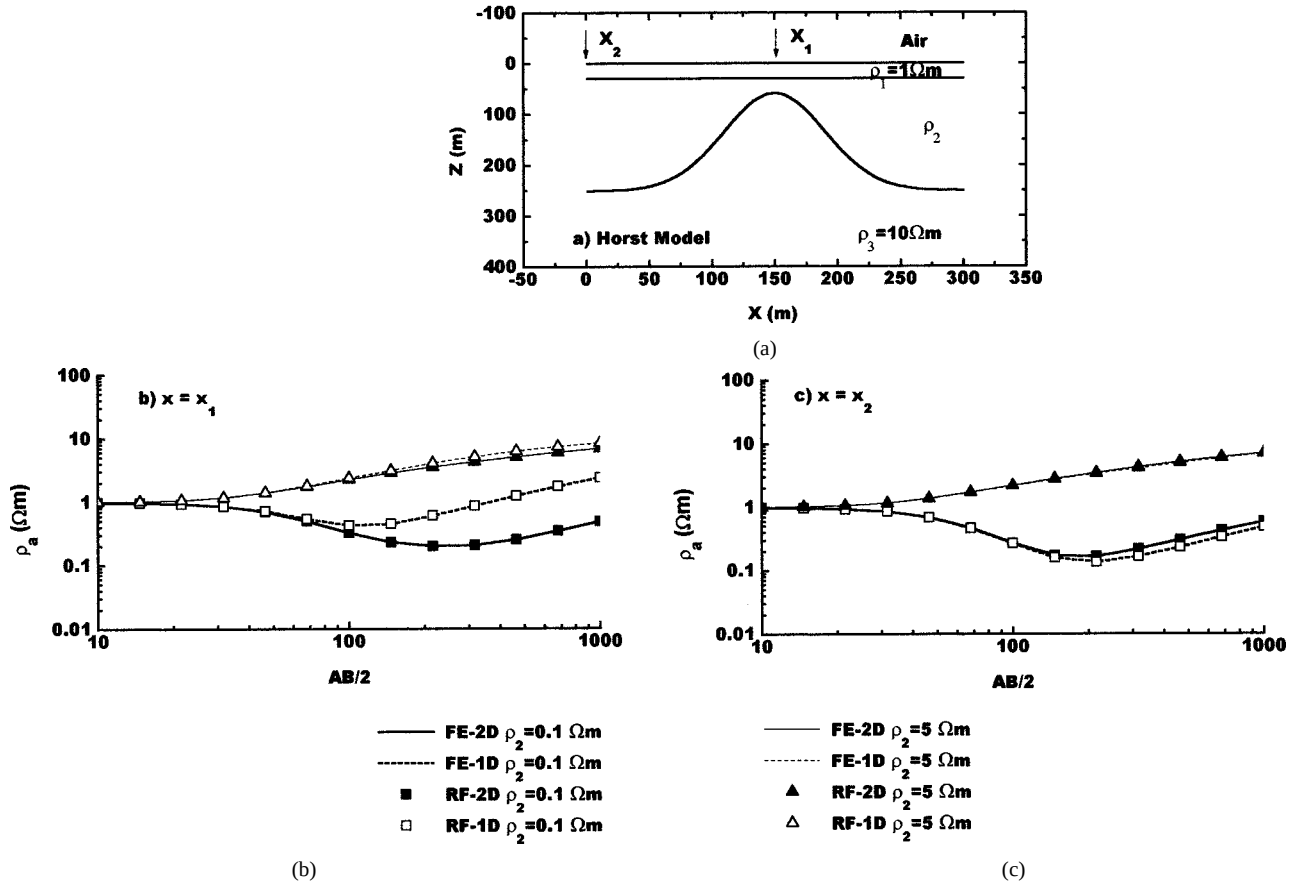

Fig. 3. (a) Horst model used to apply RF method and FE technique form [13]. x_1 and x_2 indicate the positions of two synthetic Schlumberger soundings. (b) and (c) Geoelectrical responses at x_1 and x_2, respectively, calculated with RF and FE codes assuming 2-D and 1-D layered structures.

Considering that for $l = m = 0$, only $A_{00}^{(n)} + B_{00}^{(n)}$ has a physical meaning, then

$$A_{00}^{(n)} - B_{00}^{(n)} = 0 \quad \forall n \geq 1. \tag{11}$$

When Rayleigh's approximation is valid, the series (5), (8)–(10) are convergent, so subscripts l and m can be truncated at a finite number L. Then $\phi^{(n)}$ and $\overline{J}^n$ are determined by $2(L+1)^2$ constant coefficients $A_{lm}^{(n)}$ and $B_{lm}^{(n)}$, which are calculated applying the adequate boundary conditions. On the air–earth interface $z = 0$, the vertical component of $\overline{J}$ must be null at any point other than the injection points. In addition, on every interface $z = S_n(x)$ with $1 \leq n \leq N-1$, ϕ and the normal component of $\overline{J}$ are continuous. In the last term, since the potential must not diverge when z increases, $A_{lm}^{(N)}$ must be equal to zero if l or m differ from zero. It is worthwhile to point out that the equations arising from the application of these boundary conditions can be solved separately for every m between 0 and L. The procedure employed to calculate the coefficients $A_{lm}^{(1)}$ and $B_{lm}^{(1)}$ for each m is described in the appendix.

This method has been applied to a great variety of synthetic models in order to obtain a self-consistency criterion for the determination of the validity of Rayleigh's approach in each particular case. As Rayleigh solutions are an approximation, there are residual discontinuities of ϕ and the normal component of $\overline{J}$ at layer interfaces. When the approximation is valid, the root mean square (RMS) value of these residuals can be reduced to a level below a few points per cent by increasing the number of scattering orders considered L. This is because the series are convergent. On the contrary, when the approximation is no longer valid, the residual discontinuities remain large. In these cases, either the series exhibit an oscillatory behavior or they are convergent for small values of L, and then become divergent as L increases. This consistency criterion is similar to the one found valid for the magnetotelluric 2-D and 3-D RF modeling methods [11], [12].

III. Comparison with the Finite Element Technique

To test the formulation, we calculate the geoelectric response of two different structures, a horst and a graben, and compare the results with the curves obtained using the finite element (FE) technique developed by Pous *et al.* [13]. The proposed models are shown in Figs. 3(a) and 4(a), respectively. In both cases, the lower interface is given by the following analytical function:

$$S_2 = P + D \times \exp\{-[(x - x_o)/G]^2\}$$

where $x_o = 150$ m, $G = 60$ m, and P and D are, respectively, 250 m and -190 m for the horst and 60 m and 190 m for the graben. Two values were considered for the resistivity of the second layer: ρ_2 = 0.1 Ωm and ρ_2 = 5 Ωm. These choices produce two different models, one with alternated values of the resistivity of the layers and the other with increasing ρ.

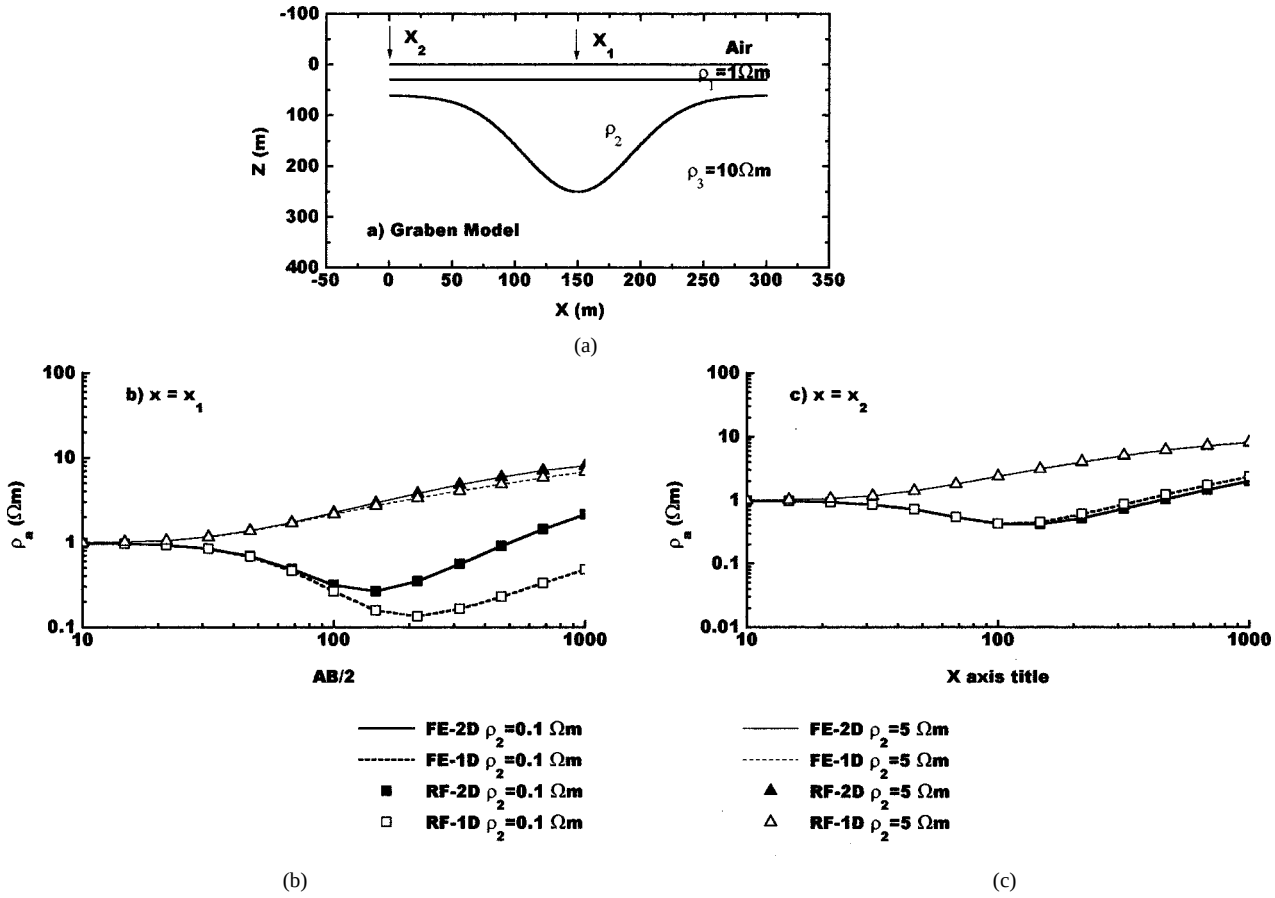

(a) (b) (c)

Fig. 4. (a) Graben model used to apply RF method and FE technique from [13]. x_1 and x_2 indicate the positions of two synthetic Schlumberger soundings. (b) and (c) Geoelectrical responses at x_1 and x_2, respectively, calculated with the RF and FE codes assuming 1-D and 2-D layered structures.

To apply the FE method, each one of these smooth models is approximated by assigning the adequate value of resistivity to every element of a rectangular mesh.

The calculations were performed at two sites, x_1 at the center of the structure and x_2 where the structure tends to recover the 1-D features. For these examples, the Schlumberger configuration was assumed for the two synthetic surveys. The curves of apparent resisitivity ρ_a versus $AB/2$ obtained by each method, for each model, at the two sites, are compared in Fig. 3(b) and (c) and in Fig. 4(b) and (c), respectively. The results obtained assuming 1-D layered structures below each site are also plotted in these figures. For both the 2-D and 1-D models, FE and RF results are in very good agreement.

For the examples analyzed here, the RF method achieved good convergence, and values of L (scattering order) lower than 15 were required in all cases. Calculation times employed to run RF and FE codes in an Digital Alpha 225 under a Unix environment were about 50 and 70 s, respectively.

We also investigated the sensitivity of the response to changes in the width of the horst and the graben by varying the value of the parameter G. Fig. 5 shows the response of each model at the site x_1 (just over the center of the anomalies), calculated for $G = 60$, 120, and 300 m. For both models, the sensitivity to the value of G obtained when $\rho_2 = 0.1\ \Omega$m is much greater than the one obtained when $\rho_2 = 5\ \Omega$m. In the first case, a splitting of the curves is clearly seen for values of $AB/2$ greater than 50 m. For other sites, the splitting diminishes as long as the distance to x_1 increases, becoming negligible for distances greater than 900 m, approximately.

IV. Discussion

An adequate imaging of subsurface structures usually requires the application of 2-D and 3-D methods to interpret geoelectrical data. Different techniques have been used, depending on the features of the structure, the geometrical configuration of the electrodes, and the extension of the surveyed area.

In particular, in this paper, we present a method that has a different applicability range from the FE or FD techniques. It is intended for the modeling of multilayered structures with irregular boundaries. The formulation is independent from the geometrical configuration of the measurement electrodes, and it is especially adequate for extended profiles. This capability was tested recently when imaging the electrical properties of an alluvial aquifer located in a Sierras Pampeanas tectonic valley [14]. In that case, a total of 17 geoelectrical depth soundings were conducted along a 35 km E-W profile, with maximum half-electrode spacing $AB/2$ of 1500 m in the Schlumberger configuration. We first interpreted the data by assuming a horizontally layered model at each sounding site using a 1-D inversion code [15]. Then, with these results, we designed a smooth starting model for the application of the RF code presented here. The

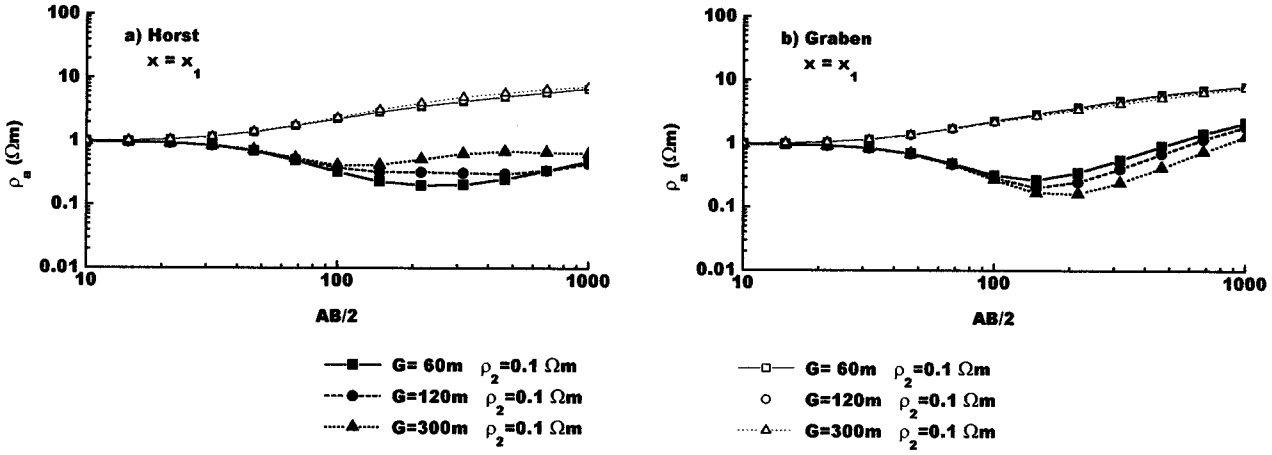

(a) (b)

Fig. 5. Dependence of the response at $x = x_1$ with the width of (a) the horst and (b) the graben, which is defined by the value of the parameter G. $G = 60$ m corresponds to the models shown in Figs. 3(a) and 4(a).

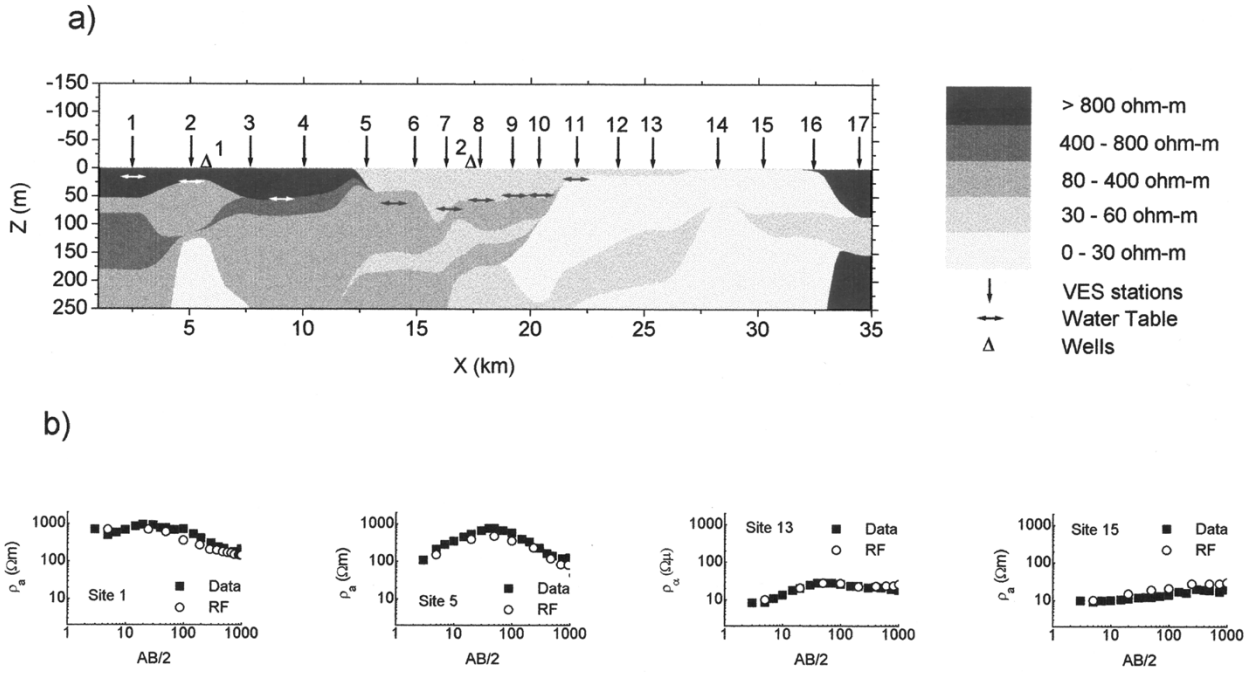

Fig. 6. (a) Electrical imaging of an alluvial aquifer in a tectonic valley, obtained using the RF code [14]. The location of the water table obtained from drillings is also indicated. (b) Response of this model compared to data obtained at various sounding sites.

final 2-D resistivity cross section obtained led to the characterization of the aquifer, whose accuracy was proved when its features were compared with the information available from ten boreholes located in that zone. The resulting electrical model of the shallow layers, together with the location of the water table, are shown in Fig. 6(a). The fittings of the apparent resistivity curves to the data at several sites are displayed in Fig. 6(b).

One of the advantages of this formulation is the friendly way to define the interfaces. Each one of them can be defined directly by an analytical function or by giving the x-z coordinates of an adequate number of points belonging to it. In the last case, the code internally generates a continuous and derivable spline function, passing through every one of these points.

APPENDIX

Here, the methodology used to calculate the coefficients $A_{lm}^{(1)}$ and $B_{lm}^{(1)}$ for every value of m is described.

On the air-earth interface $z = 0$, the vertical component of $\overline{J}$ must be null at any point other than the injection points. This condition must be imposed only to the homogeneous term $\overline{J}_H$, because it is automatically satisfied by the source term $\overline{J}_S$. Considering (8) and (11), it implies that

$$A_{lm}^{(1)} - B_{lm}^{(1)} = 0 \quad \forall (l, m). \tag{12}$$

At $z = S_n(x)$ with $1 \leq n \leq N-1$, ϕ and the normal component of $\overline{J}$ are continuous. It must be noted that the normal component of $\overline{J}$ is continuous if and only if

$$J_{\perp}(x,y,S_n(x)) = J_z(x,y,S_n(x)) - \frac{dS_n}{dx}(x) J_x(x,y,S_n(x)) \quad (13)$$

is continuous for every value of x and y between $-\lambda/2$ and $\lambda/2$. J_x and J_z are, respectively, the x and z components of $\overline{J}$.

The source terms of ϕ and $J_{\perp}$ evaluated on boundary S_1 can be expressed as

$$\phi_S(x,y,S_1(x)) = \sum_{l,m=0}^{L} V_{lm} \cos(k_l x)\cos(k_m y)) \quad (14)$$

$$J_{S\perp}(x,y,S_1(x)) = -\frac{\sigma^{(1)}}{\lambda} \sum_{l,m=0}^{L} W_{lm} \cos(k_l x)\cos(k_m y) \quad (15)$$

with

$$V_{lm} = \frac{(2-\delta_{l0})(2-\delta_{m0})}{\lambda^2} \int_{-\lambda/2}^{\lambda/2}\int_{-\lambda/2}^{\lambda/2} \phi_S(x,y,S_1(x)) \cdot \cos(k_l x)\cos(k_m y)\, dx\, dy \quad (16)$$

$$W_{lm} = -\frac{(2-\delta_{l0})(2-\delta_{m0})}{\lambda\sigma^{(1)}} \int_{-\lambda/2}^{\lambda/2}\int_{-\lambda/2}^{\lambda/2} J_{S\perp}(x,y,S_1(x)) \cdot \cos(k_l x)\cos(k_m y)\, dx\, dy. \quad (17)$$

Taking into account (5), (14), and (12), it can be demonstrated that the continuity of ϕ implies that

$$\sum_{l=0}^{L} [2A_{lm}^{(1)} \cosh(K_{lm} S_1(x)) + V_{lm}] \cos(k_l x) = \sum_{l=0}^{L} [A_{lm}^{(2)} \exp(K_{lm} S_1(x)) + B_{lm}^{(2)} \exp(-K_{lm} S_1(x))] \cos(k_l x) \quad \forall\, 0 \leq m \leq L. \quad (18)$$

Considering also (8) and (15) and doing some algebra, from the continuity of $J_{\perp}$ it is obtained that, for $m = 0$

$$\sigma^{(1)} \sum_{l=1}^{L} \left[2A_{l0}^{(1)} \sinh(k_l S_1(x)) + \frac{1}{\lambda k_l} W_{l0}\right] \sin(k_l x) = \sigma^{(2)} \sum_{l=1}^{L} [A_{l0}^{(2)} \exp(k_l S_1(x)) - B_{l0}^{(2)} \exp(-k_l S_1(x))] \sin(k_l x) \quad (19)$$

and for every $1 \leq m \leq L$

$$\sigma^{(1)} \left\{ \sum_{l=0}^{L} 2A_{lm}^{(1)} \left[K_{lm} \sinh(K_{lm} S_1(x)) \cos(k_l x) + \frac{dS_1}{dx}(x) k_l \cosh(K_{lm} S_1(x)) \sin(k_l x) \right] + \frac{1}{\lambda} \sum_{l=0}^{L} W_{lm} \cos(k_l x) \right\}$$

$$= \sigma^{(2)} \left\{ \sum_{l=0}^{L} A_{lm}^{(2)} \exp(K_{lm} S_1(x)) \left[K_{lm} \cos(k_l x) + \frac{dS_1}{dx}(x) k_l \sin(k_l x) \right] + \sum_{l=0}^{L} B_{lm}^{(2)} \exp(-K_{lm} S_1(x)) \cdot \left[-K_{lm} \cos(k_l x) + \frac{dS_1}{dx}(x) k_l \sin(k_l x) \right] \right\}. \quad (20)$$

For $z = S_n(x)$ with $2 \leq n \leq N-1$, the following equation derives from the continuity of ϕ:

$$\sum_{l=0}^{L} [A_{lm}^{(n)} \exp(K_{lm} S_n(x)) + B_{lm}^{(n)} \exp(-K_{lm} S_n(x))] \cos(k_l x) = \sum_{l=0}^{L} [A_{lm}^{(n+1)} \exp(K_{lm} S_n(x)) + B_{lm}^{(n+1)} \exp(-K_{lm} S_n(x))] \cos(k_l x) \quad \forall 0 \leq m \leq L, \quad (21)$$

while the continuity of $J_{\perp}$ gives, for $m = 0$

$$\sigma^{(n)} \sum_{l=1}^{L} [A_{l0}^{(n)} \exp(k_l S_n(x)) - B_{l0}^{(n)} \exp(-k_l S_n(x))] \sin(k_l x) = \sigma^{(n+1)} \sum_{l=1}^{L} [A_{l0}^{(n+1)} \exp(k_l S_n(x)) - B_{l0}^{(n+1)} \exp(-k_l S_n(x))] \sin(k_l x) \quad (22)$$

and, for $1 \leq m \leq L$

$$\sigma^{(n)} \left\{ \sum_{l=0}^{L} A_{lm}^{(n)} \exp(K_{lm} S_n(x)) \cdot \left[K_{lm} \cos(k_l x) + \frac{dS_n}{dx}(x) k_l \sin(k_l x) \right] + \sum_{l=0}^{L} B_{lm}^{(n)} \exp(-K_{lm} S_n(x)) \cdot \left[-K_{lm} \cos(k_l x) + \frac{dS_n}{dx}(x) k_l \sin(k_l x) \right] \right\}$$

$$= \sigma^{(n+1)} \left\{ \sum_{l=0}^{L} A_{lm}^{(n+1)} \exp(K_{lm} S_n(x)) \cdot \left[K_{lm} \cos(k_l x) + \frac{dS_n}{dx}(x) k_l \sin(k_l x) \right] + \sum_{l=0}^{L} B_{lm}^{(n+1)} \exp(-K_{lm} S_n(x)) \cdot \left[-K_{lm} \cos(k_l x) + \frac{dS_n}{dx}(x) k_l \sin(k_l x) \right] \right\}. \quad (23)$$

As the potential must not diverge when z increases

$$A_{lm}^{(N)} = 0 \quad \forall (l,m) \neq (0,0). \quad (24)$$

It can be noted that the equations arising from the application of boundary conditions can be solved separately for every m between 0 and L. This is an important consequence of the bidimensionality of the structure that simplifies the resolution procedure and reduces calculation times.

In order to obtain a unique solution, a system of $2(L+1)$ linearly independent equations is required for each inteface S_n with $1 \leq n \leq N-1$. These systems are built-up evaluating the equations arising from the application of boundary conditions at the following $L+1$ equally-spaced points x_i:

$$x_i = \frac{i\lambda}{2L+1} \quad \text{for } 0 \leq i \leq L. \tag{25}$$

For the interfaces S_n with $2 \leq n \leq N-1$, if $m > 0$, then (21) and (23) are evaluated at the points x_0 to x_L. On the other hand, when $m = 0$, then (21) is evaluated at the points x_0 to x_L, (22) is evaluated at x_1 to x_L, and the relation (11) is considered. This leads to the following matrix systems:

$$\mathbf{M1}^{(n)}(\overline{A}^{(n)} - \overline{A}^{(n+1)}) + \mathbf{M2}^{(n)}(\overline{B}^{(n)} - \overline{B}^{(n+1)}) = 0 \tag{26}$$

$$\mathbf{P1}^{(n)}(\sigma^{(n)}\overline{A}^{(n)} - \sigma^{(n+1)}\overline{A}^{(n+1)}) + \mathbf{P2}^{(n)}(\sigma^{(n)}\overline{B}^{(n)} - \sigma^{(n+1)}\overline{B}^{(n+1)}) = 0 \tag{27}$$

$$\mathbf{P1}^{(n)}(\sigma^{(n)}\overline{A}^{(n)} - \sigma^{(n+1)}\overline{A}^{(n+1)}) + \mathbf{P2}^{(n)}(\sigma^{(n)}\overline{B}^{(n)} - \sigma^{(n+1)}\overline{B}^{(n+1)}) = 0 \tag{27}$$

where the vectors $\overline{A}^{(n)}$ and $\overline{B}^{(n)}$ are defined for every l between 0 and L as

$$\{\overline{A}^{(n)}\}_l = A_{lm}^{(n)} \quad \{\overline{B}^{(n)}\}_l = B_{lm}^{(n)} \tag{28}$$

and $\forall\, 0 \leq i, l \leq L$

$$\{\mathbf{M1}^{(n)}\}_{il} = \exp(K_{lm}S_n(x_i))\cos(k_l x_i) \tag{29}$$

$$\{\mathbf{M2}^{(n)}\}_{il} = \exp(-K_{lm}S_n(x_i))\cos(k_l x_i) \tag{30}$$

If $m = 0$, $\mathbf{P1}^{(n)}$ and $\mathbf{P2}^{(n)}$ take the form $\forall\, 0 \leq i, l \leq L$

$$\{\mathbf{P1}^{(n)}\}_{il} = \delta_{i0}\delta_{l0} + \exp(k_l S_n(x_i))\sin(k_l x_i) \tag{31}$$

$$\{\mathbf{P2}^{(n)}\}_{il} = -[\delta_{i0}\delta_{l0} + \exp(-k_l S_n(x_i))\sin(k_l x_i)] \tag{32}$$

while if $0 < m \leq L$, then $\forall\, 0 \leq i, l \leq L$

$$\{\mathbf{P1}^{(n)}\}_{il} = \lambda \exp(K_{lm}S_n(x_i)) \cdot \left[K_{lm}\cos(k_l x_i) + \frac{dS_n}{dx}(x_i)k_l \sin(k_l x_i)\right] \tag{33}$$

$$\{\mathbf{P2}^{(n)}\}_{il} = \lambda \exp(-K_{lm}S_n(x_i)) \cdot \left[-K_{lm}\cos(k_l x_i) + \frac{dS_n}{dx}(x_i)k_l \sin(k_l x_i)\right]. \tag{34}$$

Taking into account equations (11) and (24), then

$$\{\overline{A}^{(N)}\}_l = \delta_{l0}\delta_{m0}B_{00}^{(N)} \quad \forall\, 0 \leq l \leq L. \tag{35}$$

Solving (26) and (27) from the lower interface to the second one, a relation is obtained between $\overline{A}^{(2)}$ and $\overline{B}^{(2)}$

$$\overline{A}^{(2)} = \mathbf{Mat}^{(2)}\overline{B}^{(2)} \tag{36}$$

where $\mathbf{Mat}^{(2)}$ only depends on the characteristics of the structure and not on the geometry of the sources.

Finally, at $z = S_1(x)$, (18) is evaluated at the points x_0 to x_L. In addition, if $m = 0$, (19) is evaluated at x_1 to x_L, and the relation (11) is considered. For the other case $0 < m \leq L$, (20) is evaluated at x_0 to x_L. Considering (36), the systems obtained are

$$\mathbf{M0}\,\overline{A}^{(1)} + \mathbf{MS}\,\overline{V} - (\mathbf{M1}^{(1)}\mathbf{Mat}^{(2)} + \mathbf{M2}^{(1)})\overline{B}^{(2)} = 0 \tag{37}$$

$$\sigma^{(1)}(2\mathbf{P0}\,\overline{A}^{(1)} + \mathbf{PS}\,\overline{W}) - \sigma^{(2)}(\mathbf{P1}^{(1)}\mathbf{Mat}^{(2)} + \mathbf{P2}^{(1)})\overline{B}^{(2)} = 0 \tag{38}$$

with $\mathbf{M1}^{(1)}$ and $\mathbf{M2}^{(1)}$ defined, respectively, by (29) and (30), and

$$\{\mathbf{M0}\}_{il} = \cosh(K_{lm}S_1(x_i))\cos(k_l x_i) \tag{39}$$

$$\{\mathbf{MS}\}_{il} = \cos(k_l x_i) \tag{40}$$

for $0 \leq i, l \leq L$.

If $m = 0$

$$\{\mathbf{P0}\}_{il} = \sinh(k_l S_1(x_i))\sin(k_l x_i) \tag{41}$$

$$\{\mathbf{PS}\}_{il} = \frac{1}{\lambda k_l}\sin(k_l x_i) \tag{42}$$

$$\{\mathbf{P1}^{(n)}\}_{il} = \exp(k_l S_1(x_i))\sin(k_l x_i) \tag{43}$$

$$\{\mathbf{P2}^{(n)}\}_{il} = -\exp(-k_l S_1(x_i))\sin(k_l x_i) \tag{44}$$

for $1 \leq i, l \leq L$.

In the other case, $m > 0$, $\mathbf{P1}^{(1)}$, and $\mathbf{P2}^{(1)}$ are given by (33) and (34), and

$$\{\mathbf{P0}\}_{il} = \lambda\left[K_{lm}\sinh(K_{lm}S_1(x_i))\cos(k_l x_i) + \frac{dS_1}{dx}(x_i)k_l\cosh(K_{lm}S_1(x_i))\sin(k_l x_i)\right] \tag{45}$$

$$\{\mathbf{PS}\}_{il} = \{\mathbf{MS}\}_{il} = \cos(k_l x_i) \tag{46}$$

for $0 \leq i, l \leq L$.

From (37) and (38), the vector $\overline{A}^{(1)}$ can be calculated for every value of m.

It must be noted that relation (38) gives $L+1$ equations when $m > 0$, but only L equations when $m = 0$. This is correct because of the fact that $A_{00}^{(1)} = B_{00}^{(1)}$ is implicitly included in relation (37).

REFERENCES

[1] T. Lee, "An integral equation and its solution for some two and three dimensional problems in resistivity and induced polarization," *Geophysics*, vol. 42, pp. 81–95, 1975.

[2] U. C. Das and D. S. Parasnis, "Resistivity and induced polarization responses of arbitrarily shaped 3-D bodies in a two-layered earth," *Geophys. Prospect.*, vol. 35, pp. 98–109, 1987.

[3] J. H. Coggon, "Electromagnetic and electrical modeling by a finite element method," *Geophysics*, vol. 36, pp. 106–136, 1971.

[4] D. Pridmore, G. W. Hohmann, S. H. Ward, and W. R. Sill, "An investigation of finite element modeling for electrical and electromagnetic modeling data in three dimensions," *Geophysics*, vol. 46, pp. 1009–1024, 1981.

[5] P. Queralt, J. Pous, and A. Marcuello, "2D resistivity modeling: An approach to arrays parallel to the strike directo," *Geophysics*, vol. 56, pp. 941–950, 1991.

[6] I. R Mufti, "Finite-difference resistivity modeling for arbitrarily shaped two-dimensional structure," *Geophysics*, vol. 41, pp. 62–78, 1976.

[7] A. Dey and H. F. Morrison, "Resistivity modeling for arbitrarily shaped three-dimensional structures," *Geophysics*, vol. 44, pp. 753–780, 1979.

[8] T. Lowry, M. B. Allen, and P. N. Shive, "Singularity removal: A refinement of resistivity modeling technique," *Geophysics*, vol. 54, pp. 766–744.

[9] S. Zhao and M. Yedlin, "Some refinements on the finite-difference method for 3-D dc resistivity modeling," *Geophysics*, vol. 61, pp. 1301–1307, 1996.
[10] J. Zhang, R. L. Mackie, and T. R. Madden, "3-D resistivity forward modeling and inversion using conjugate gradients," *Geophysics*, vol. 60, pp. 1313–1325, 1995.
[11] A. Osella and P. Martinelli, "Magnetotelluric response of anisotropic 2-D structures," *Geophys. J. Int.*, vol. 115, pp. 819–828, 1993.
[12] P. Martinelli and A. Osella,, "MT forward modeling of 3-D anisotropic electrical conductivity structures using the Rayleigh-Fourier method," *J. Geomagn. Geoelectron.*, vol. 49, pp. 1499–1518, 1997.
[13] J. Pous, P. Queralt, and R. Chavez, "Lateral and topographic effects in geoelectric soundings," *J. Appl. Geophys.*, vol. 35, pp. 237–248, 1996.
[14] A. Osella, A. Favetto, P. Martinelli, and D. Cernadas, "Electrical imaging of an alluvial aquifer at the Antinaco-Los Colorados tectonic valley in the Sierras Pampeanas, Argentina," *J. Appl. Geophys.*, vol. 41, pp. 359–368, 1998.
[15] D. L. Jupp and K. Vozoff, "Stable iterative methods for the inversion of geophysical data," *Geophys. J. R. Astron. Soc.*, vol. 42, pp. 957–976, 1975.

Ana Osella received the Ph.D. degree in physics from the University of Buenos Aires, Buenos Aires, Argentina, in 1983.

She has been a Research Scientist in the Consejo Nacional de Investigaciones Científicas y Técnicas (CONICET) and a Professor with the Faculty of Sciences, University of Buenos Aires, since 1984. Since 1988, she has been Head of the Applied Geophysics Group. Her research interests include the fields of electromagnetic (EM) induction in the earth, EM and DC measurements for upper crustal studies and to environmental and engineering applications, continental lower crustal studies through EM data, and seismicity.

Patricia Martinelli received the Ph.D. degree in physics from the University of Buenos Aires, Buenos Aires, Argentina, in 1994.

She is an Associate Research Scientist in the Consejo Nacional de Investigaciones Científicas y Técnicas (CONICET) and a member of the Physics Department of the Faculty of Sciences, University of Buenos Aires. Her main research interests include the development of 2-D and 3-D electromagnetic modeling codes and the study of the electrical properties of the crust and upper mantle in the South American subduction zone.

Daniel Cernadas received the degree in physics from the University of Buenos Aires, Buenos Aires, Argentina, in 1997.

He is a member of the Physics Department, Faculty of Sciences, University of Buenos Aires. His research interests include modeling and interpretation of DC data and the analysis of seismic data from the Andean subduction zone.